TECHNICAL UNIVERSITY OF CLUJ-NAPOCA

ACTA TECHNICA NAPOCENSIS

Series: Applied Mathematics, Mechanics, and Engineering
Vol. 69, Issue II, June, 2026

ADAPTIVE PERIMETERS GENERATION FOR FUSED FILAMENT FABRICATION: EVALUATION OF ARACHNE ALGORITHM

Alexandru Ionuț IRIMIA, Ionuț Mădălin PIȘTA, Marius Ionuț RÎPANU, Vasile MERTICARU, Marius-Andrei MIHALACHE, Vasile ERMOLAI

Abstract: *In Fused Filament Fabrication (FFF), the perimeter toolpath strategy strongly influences dimensional accuracy of the resulting components. The Arachne algorithm varies extrusion width along each perimeter through a medial-axis beading strategy, adapting to local wall geometry, whereas the Classic algorithm holds the contour width fixed. We compared the two algorithms experimentally on a purpose-designed L-benchmark with wall thicknesses varying from 1 to 5 mm, printed at three nozzle diameters (0.4, 0.6, and 0.8 mm) on a Bambu Lab A1 in PolyTerra PLA. Across 270 micrometer measurements, Arachne reduced mean absolute error by 2.3 to 7.0 times and maintained 100% of features within ±0.1 mm of nominal across all nozzle sizes, while Classic achieved only 78% (0.6 mm) and 89% (0.8 mm). Print-time and material-consumption differences stayed below 1.2% and 1.8%, respectively, confirming negligible production cost.*

Key words: *Arachne algorithm, perimeter toolpath generation, Fused Filament Fabrication, dimensional accuracy, process capability.*

1. INTRODUCTION

Fused Filament Fabrication (FFF) has become a widely adopted additive manufacturing technology for rapid prototyping and small-batch production of thermoplastic polymeric parts [1–3]. Despite this accessibility, the dimensional accuracy of FFF parts continues to attract active investigation. Process parameters such as layer height, raster width, build orientation, and print speed all influence the final geometry [4, 5]. Among these, the slicer's perimeter toolpath strategy stands out as a particularly important yet often underappreciated variable, because it determines how closely the deposited material conforms to the nominal cross-section of each wall feature.

Conventional slicing algorithms employ a uniform contour-offset approach: the nozzle traces concentric contours at a fixed extrusion width, typically close to the nominal nozzle diameter [6]. However, prior work has shown that the extrusion width can reach up to 260% of the nozzle diameter [7]. When a wall thickness is an exact integer multiple of the line width, this strategy works well. When wall thickness falls between integer multiples, however, the slicer either leaves an unfilled gap between the innermost perimeters or forces a thin extra perimeter at excessive overlap, producing inter-layer voids and dimensional error [8]. Jiang and Ma [6] reviewed path planning strategies for additive manufacturing and confirmed that contour-parallel methods with constant line spacing are prone to under- and over-filling at non-integer wall thicknesses. Altiparmak et al. [9] further identified toolpath-induced voids as a persistent limitation of extrusion-based processes, noting that adaptive-width strategies represent a promising way for improvement.

Kuipers et al. [1] introduced the Arachne framework to address this fundamental limitation. Arachne adopts a medial-axis-based slicing strategy that varies each perimeter's extrusion width within a controlled range (0.75w to 1.5w for a nozzle of diameter w). Instead of forcing uniform-width contours and accepting the resulting underfill or overfill, Arachne computes a variable-width toolpath that fully tessellates the cross-section while

Received: 28.04.26; **Similarities**: 16.04.26: **Reviewed**: 28.04. 28.04.26: **Accepted 1**5.06.26.

keeping every bead inside the extruder's reliable operating envelope. The theoretical foundation for variable-width contouring was further developed by Hornus et al. [10], who formulated the bead-width selection as an optimization problem on the medial axis transform, and by Ding et al. [11], who proposed a process planning framework for adaptive contour-parallel toolpaths with variable bead widths in additive manufacturing of lightweight thin-wall structures. Related work by Kuipers et al. [12] on the CrossFill infill structure demonstrated the benefits of adaptive subdivision for generating continuous, overlap-free extrusion paths. Cura adopted the Arachne algorithm in version 5.0, and Bambu Studio, Orca Slicer, and Prusa Slicer have since followed.

Sun et al. [8] reviewed the sources of voids in material-extrusion additive manufacturing, classifying them into inter-layer (or inter-track), intra-layer (or intra-track), underfill, and surface voids. Their analysis confirms that non-tessellating bead cross-sections and geometry-dependent gap formation are primary contributors to reduced mechanical properties and poor surface finish. Mohamed et al. [13] conducted an earlier comprehensive review of FFF process optimization, identifying that raster width and air gap are among the most influential parameters affecting part quality; parameters that Arachne modifies dynamically. Sood et al. [4] demonstrated through experimental design that dimensional accuracy in FFF is governed by complex interactions among five process parameters, with raster width deviations producing the largest effects on measured wall thickness. Allum et al. [14] investigated the filament-scale geometry of FFF thin-walled specimens and showed that wall thicknesses not matching integer multiples of the deposited bead width develop systematic inter-layer voids and dimensional deviations, a finding that directly motivates the experimental evaluation of adaptive perimeter generation undertaken in the present study.

Although prior work has demonstrated Arachne's benefits computationally [1, 10, 11], independent experimental validation on physically printed parts remains scarce. Most published studies on FFF dimensional accuracy optimize conventional process parameters (e.g., temperature, speed, layer height) rather than treating the slicer's perimeter algorithm as an independent variable. This study delivers a systematic experimental comparison of the Classic (i.e., uniform-offset) and Arachne (i.e., adaptive-width) perimeter generation algorithms on a purpose-designed benchmark part. Wall features from 1 mm to 5 mm were printed at three nozzle diameters (0.4, 0.6, and 0.8 mm) and measured with a digital micrometer. The objectives are: (1) to quantify the dimensional accuracy and precision of each algorithm across the full feature-size range; (2) to evaluate the effect of nozzle diameter on algorithm performance; (3) to assess the practical trade-offs in print time and material consumption; and (4) to provide photographic evidence of top surface-level printing defects associated with each algorithm.

2. MATERIAL AND METHODS

2.1 Benchmark test piece

The benchmark geometry (Fig. 1) was designed as a rectangular plate of approximately 185 × 95 × 5 mm containing nine L-shaped extruded features of 20 mm with nominal wall thicknesses of 1 mm to 5 mm.

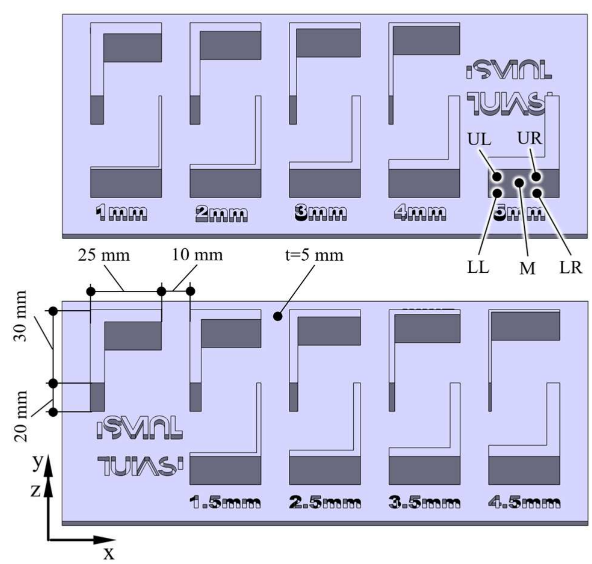

Fig. 1. Wall-thickness benchmark, with nine L-shaped pockets ranging from 1 to 5 mm in 0.5 mm steps and embossed/debossed nominal-size labels of 3 mm height.

A text-label region on the in the front side carries the wall thickness nominal-size. Each feature comprises two perpendicular walls forming an L-shaped cross-section, which permits wall-thickness measurements at five positions per side (next to the embossed/debossed label): lower-left (LL), lower-right (LR), middle (M), upper-right (UR), and upper-left (UL). The geometry was modelled in Free CAD 1.1, exported as a STEP file, and imported into Orca Slicer for toolpath generation.

2.2 Printing equipment and parameters

All specimens were fabricated on a Bambu Lab A1 desktop FFF printer using PolyTerra PLA (Polymaker), a bio-based PLA blend. Three nozzle diameters were evaluated: 0.4, 0.6, and 0.8 mm.

Table 1

Printing process parameters.

No.		Parameter	Value
1		Nozzle diameter (mm)	0.4/*0.6*/**0.8**
2		Layer thickness (mm)	0.24
3		Extrusion width (mm)	0.4/*0.6*/**0.8**
4		Number of walls	13
5		Wall generator	Classic (a)
			Arachne (b)
	5.1b	Wall transition threshold angle (°)	10
	5.2b	Wall transition filter margin (%)	25
	5.3b	Wall transition length (%)	100
	5.4b	Wall distribution count	2
	5.5b	Minimum wall width (%)	85
	5.6b	Minimum feature size (%)	25
	5.7b	Minimum wall width (mm)	0.5
6		Top/bottom layers	4
		Infill pattern	Grid
		Infill density (%)	30
		First layer printing speed (mm/s)	50
5		Walls printing speed (mm/s)	100
6		Other layers printing speed (mm/s)	150
7		Extrusion temperature (°C)	220
8		Maximum fan speed (%)	80
9		Bed temperature (°C)	65
11		Z seam position	Aligned
12		Brim	Yes
13		Brim width (mm)	5
14		Retraction distance (mm)	0.8
15		Retraction speed (mm/s)	30
16		Z hop height (mm)	0.4

Values in italic apply to 0.6 mm nozzle;
Values in bold apply to 0.8 mm nozzle.

For each nozzle, two specimens were printed under identical process conditions, the only difference being the perimeter generation algorithm: Classic (i.e., uniform offset contours with line width equal to the nozzle diameter) and Arachne (i.e., adaptive extrusion width, after Kuipers et al. [1]). Slicing was performed in Orca Slicer 2.3.2-beta, which integrates the Arachne engine from lib Arachne. The L-shaped features were printed without top layers to evaluate the slicing algorithm susceptibility inner-layer void formation. All remaining print settings (listed in Table 1) were held constant across the six prints. The full experimental set-up therefore comprised six sample (3 nozzles × 2 algorithms), requiring approximately 13.5 h of cumulative print time and 612 g of filament.

2.3 Measurement procedure

Wall thicknesses were measured with a Beslands digital micrometer having a resolution 0.001 mm. Each of the nine wall features was measured at the five positions defined in section 2.1, giving 45 readings per specimen and 270 readings. All measurement were done in a single run, in a controlled environment having 18°C and 38% relative humidity All measurements were taken near the boundary of each wall segment to avoid edge effects. For every nozzle–algorithm combination and feature size, the mean, standard deviation, bias (mean – nominal), absolute error, and percentage error were determined. Process-capability indices Cp and Cpk were calculated under a bilateral tolerance band of ±0.1 mm about the nominal (USL = nominal + 0.1, LSL = nominal – 0.1).

2.4 Statistical analysis

Three statistical tests were applied per nozzle diameter. A paired t-test compared the absolute errors of the two algorithms across the nine feature sizes (H_0: mean |error| is identical for both algorithms). An F-test compared the variances of those absolute errors (H_0: variances are equal), serving as an indicator of process consistency. Finally, a linear regression of measured mean against nominal dimension was fitted for each nozzle–algorithm combination; the slope deviation from unity quantifies systematic scaling error, while R^2 captures linearity. A significance level of $\alpha = 0.05$ was used throughout.

3. RESULTS AND DISCUSSION

The Results section is organized as follows. Figures 2–7 present, for each nozzle diameter, side-by-side comparisons of the slice preview and the printed specimen for the Classic and Arachne algorithms, using the 3.5 mm feature as a representative wall thickness.

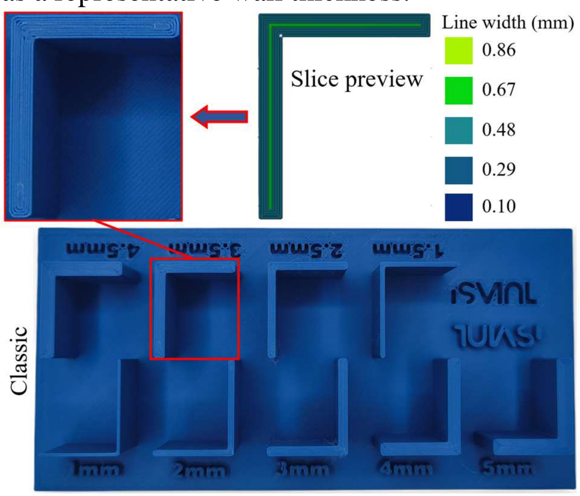

Fig. 2. Benchmark printed with the Classic algorithm and a 0.4 mm nozzle. Inset: slice preview and resulting geometry of the 3.5 mm feature.

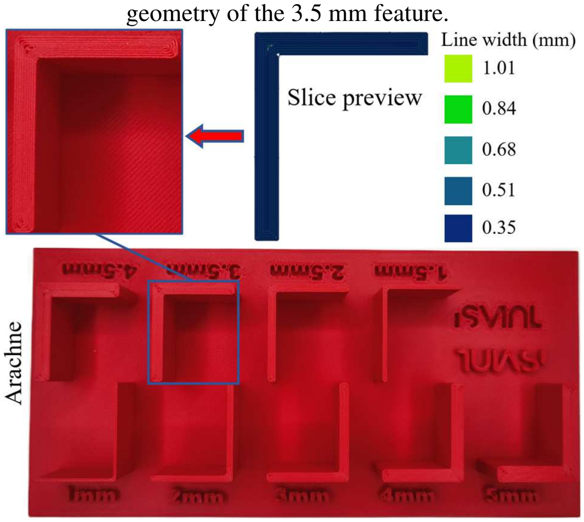

Fig. 3. Benchmark printed with the Arachne algorithm and a 0.4 mm nozzle. Inset: slice preview and resulting geometry of the 3.5 mm feature.

Quantitative dimensional accuracy is then analyzed in section 3.1 (Table 2, Fig. 11), regression behavior in section 3.2 (Table 3), precision and process capability in section 3.3 (Table 4), statistical significance in section 3.4 (Tables 5 and 6), and print time and material consumption in section 3.5 (Figs. 12 and 13).

The Classic generator at the 0.4 mm nozzle (Fig. 2) sets the baseline for uniform-offset behavior at fine extrusion widths. At the same nozzle, Arachne (Fig. 3) fills the same 3.5 mm wall feature with adaptive bead widths, exposing the contrast directly.

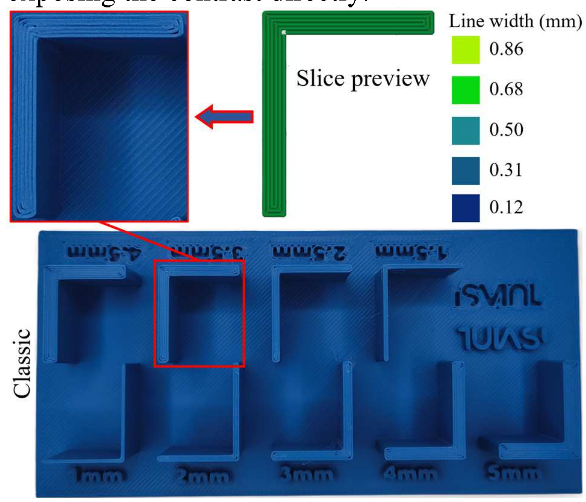

Fig. 4. Benchmark printed with the Classic algorithm and a 0.6 mm nozzle. Inset: slice preview and resulting geometry of the 3.5 mm feature.

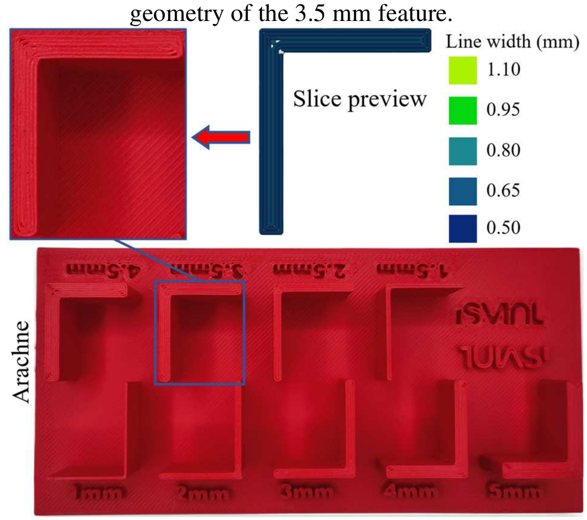

Fig. 5. Benchmark printed with the Arachne algorithm and a 0.6 mm nozzle. Inset: slice preview and resulting geometry of the 3.5 mm feature.

At 0.6 mm, the Classic strategy amplifies the mismatch between feature size and line width, with corner voids becoming more pronounced (Fig. 4). Arachne redistributes bead widths across the cross-section and shrinks the inter-layer gaps (Fig. 5), although residual voids persist where the toolpath changes direction.

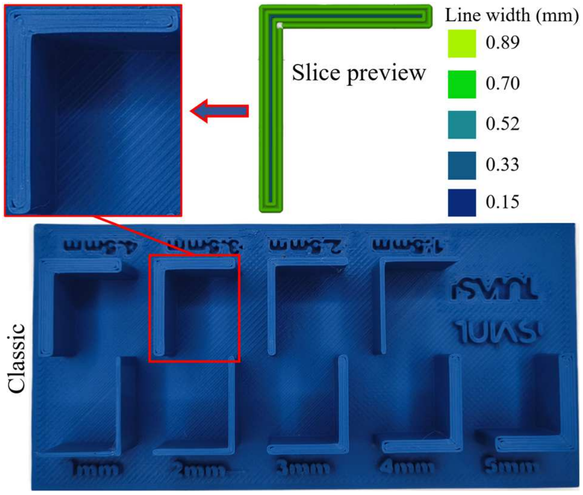

Fig. 6. Benchmark printed with the Classic algorithm and a 0.8 mm nozzle. Inset: slice preview and resulting geometry of the 3.5 mm feature.

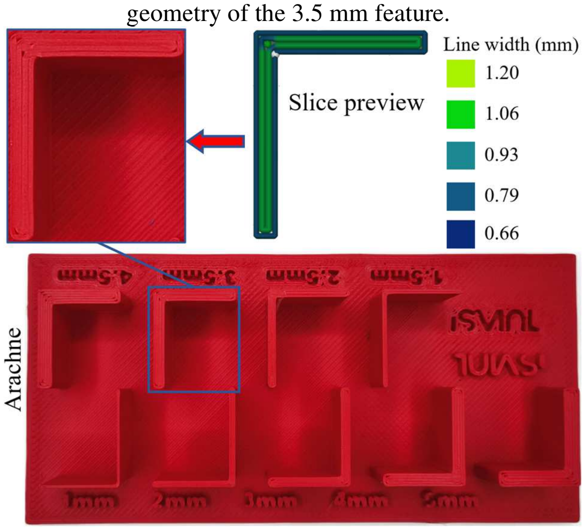

Fig. 7. Benchmark printed with the Arachne algorithm and a 0.8 mm nozzle. Inset: slice preview and resulting geometry of the 3.5 mm feature.

At the largest nozzle, Classic must trade an unfilled internal gap against an over-compressed final perimeter on the 3.5 mm wall (Fig. 6), whereas Arachne fills the same wall with a small number of variable-width beads that conform to the local geometry (Fig. 7). Wider extrusion at this nozzle nonetheless enlarges the corner voids in both cases.

3.1 Dimensional accuracy

Aggregated measurements for the 0.4 mm nozzle are plotted against nominal wall thickness to compare the linearity and scatter of the two algorithms, as shown in Fig. 8.

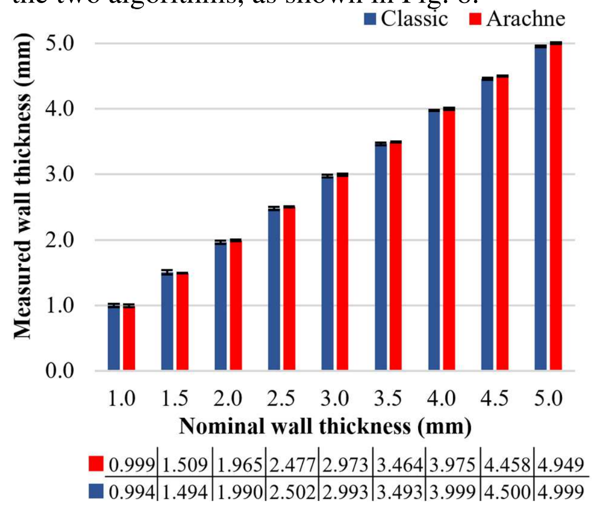

Fig. 8. Mean measured wall thickness versus nominal value for the 0.4 mm nozzle, comparing the Classic and Arachne algorithms.

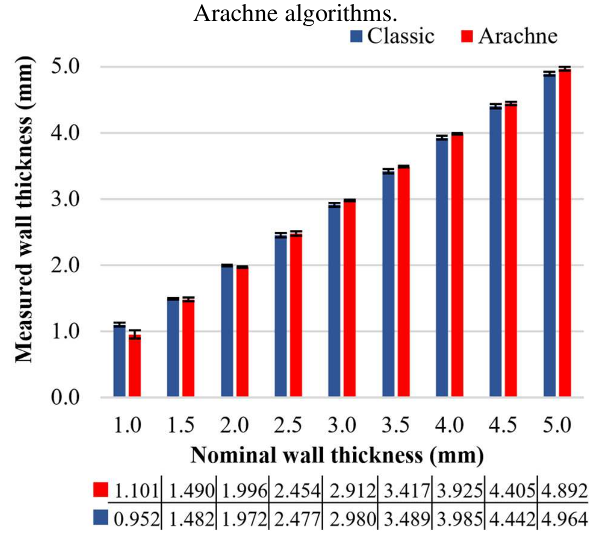

Fig. 9. Mean measured wall thickness versus nominal value for the 0.6 mm nozzle.

The same measured-versus-nominal comparison is repeated at the 0.6 mm nozzle, where the Classic curve begins to deviate visibly from the unity line at several feature sizes, as shown in Fig. 9.

At the 0.8 mm nozzle, the measured-versus-nominal trend exposes the largest systematic undersizing of the Classic algorithm and a clear outlier at the 1 mm wall, as shown in Fig. 10. Aggregated accuracy metrics for each nozzle-algorithm combination are reported in Table 2 and visualized per nozzle in Figs. 8–10, with the cross-nozzle comparison of MAE shown in Fig. 11.

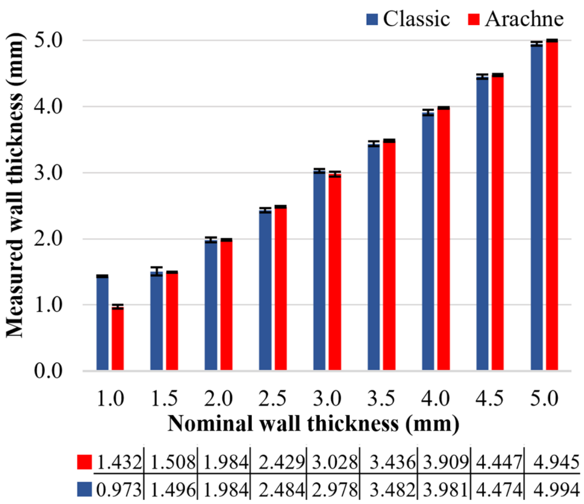

Fig. 10. Mean measured wall thickness versus nominal value for the 0.8 mm nozzle.

Table 2

Aggregated error metrics per configuration.

Noz-zle	Algo-rithm	MAE (mm)	RMSE (mm)	Mean Bias (mm)	Max |Err| (mm)	% within ±tol
0.4	Classic	0.028	0.031	-0.026	0.051	100.0%
0.4	Arachne	0.004	0.005	-0.004	0.010	100.0%
0.6	Classic	0.068	0.077	-0.045	0.108	77.8%
0.6	Arachne	0.029	0.032	-0.029	0.058	100.0%
0.8	Classic	0.091	0.153	+0.013	0.432	88.9%
0.8	Arachne	0.017	0.019	-0.017	0.027	100.0%

Arachne outperformed the Classic algorithm at every nozzle diameter. With the 0.4 mm nozzle, the Mean Absolute Error (MAE) fell from 0.028 mm with Classic to 0.004 mm with Arachne; a roughly seven-fold improvement. The advantage was preserved at larger nozzles: MAE dropped from 0.068 to 0.029 mm at 0.6 mm and from 0.091 to 0.017 mm at 0.8 mm. Arachne outperformed the Classic algorithm at every nozzle diameter. Root Mean Square Error (RMSE) followed the same pattern, with Arachne values 2–8 times lower than Classic in every configuration. The slice-preview and printed-part details in Figs. 2–7 reveal the geometric origin of these differences: at each nozzle size, the Classic toolpath either leaves visible inter-layer voids or forces an oversized final perimeter at the 3.5 mm feature, whereas the Arachne toolpath fills the cross-section continuously with smoothly varying bead widths.

Arachne held 100% of features within the ±0.1 mm tolerance band at all three nozzle sizes; Classic dropped to 78% at 0.6 mm and 89% at 0.8 mm (Table 2). Classic produced severe local deviations at specific feature sizes, visible as outliers in Figs. 8–10: the 1 mm wall at the 0.8 mm nozzle was printed at a +0.432 mm bias (measured 1.432 mm, a 43% oversize), and the 1 mm and 5 mm walls at the 0.6 mm nozzle were the two features outside the ±0.1 mm tolerance band, exhibiting biases of +0.101 mm (measured 1.101 mm) and –0.108 mm (measured 4.892 mm), respectively (Table 4). These two cases correspond to feature-to-nozzle ratios of 1.25 and 1.67; geometries at which the uniform-offset strategy must trade an internal gap against an over-compressed perimeter, consistent with the underfill and overfill mechanisms identified by Kuipers et al. [1] and reviewed by Sun et al. [8].

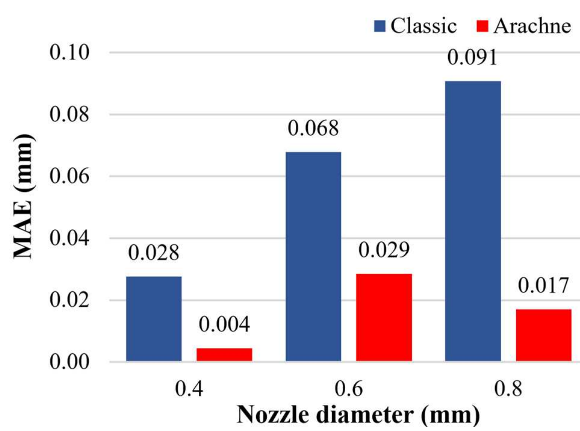

Fig. 11. Mean Absolute Error (MAE) of measured wall thickness for the Classic and Arachne algorithms at each of the three nozzle diameters.

3.2 Regression analysis

Linear regression of measured mean against nominal dimension (Table 3) shows the Classic slope drifting progressively from unity as nozzle diameter rises: 0.989 (0.4 mm), 0.958 (0.6 mm), and 0.924 (0.8 mm), which is a systematic undersizing that worsens at roughly 1.6% per 0.1 mm of nozzle increase. Arachne, by contrast, holds near-perfect linearity with slopes of 1.002, 0.999, and 1.000 and $R^2 \geq 0.9999$ across the three nozzle sizes. Classic R^2 degrades to 0.991 at 0.8 mm, mirroring the scatter from the outlier feature sizes discussed in section 3.1. The adaptive extrusion-width strategy therefore compensates directly for the geometric mismatch between feature size and nozzle diameter that drives Classic's scaling error.

Table 3

Linear regression: Measured = a + b · Nominal (per configuration). Ideal: slope b = 1, intercept a = 0, R^2 = 1. Slope deviation indicates *systematic scaling error.*

Config.	Slope	Intercept	R^2	Slope error %
0.4 Classic	0.988	+0.0088	0.9999	-1.15%
0.4 Arachne	1.001	-0.0086	1.0000	+0.16%
0.6 Classic	0.957	+0.0822	0.9994	-4.25%
0.6 Arachne	0.998	-0.0253	0.9999	-0.11%
0.8 Classic	0.924	+0.2404	0.9905	-7.57%
0.8 Arachne	1.000	-0.0179	1.0000	+0.03%

3.3 Precision and process capability

Beyond accuracy, Arachne also delivered superior consistency (Table 4). At the 0.4 mm nozzle, every Arachne Cpk exceeded 1.33, the conventional threshold for a capable process, with values from 1.63 to 6.79; Classic Cpk spanned 0.87 to 2.26 and fell below 1.0 at several feature sizes. The gap widened at larger nozzles: several Classic configurations at 0.6 mm and 0.8 mm returned negative Cpk, placing the mean outside the ±0.1 mm tolerance interval, whereas Arachne held Cpk > 0.28 even in its worst case (the 1 mm wall at the 0.6 mm nozzle, whose feature-to-nozzle ratio of 1.67 is the most challenging in the test matrix). Averaged across all 27 configurations, the coefficient of variation (CV) reached 0.94% for Arachne against 1.1% for Classic, confirming that adaptive extrusion width yields not only smaller errors but also more repeatable ones.

Table 4

Precision and process capability. n=5 per cell. CV = StDev/Mean. Bias = mean – nominal. Cp/Cpk use USL=Nominal+tol, LSL=Nominal-tol.

Nzl.	Algo.	Nom	Mean	Bias (mm)	St. Dev.	CV (%)	Cp	Cpk
0.4	Classic	1	0.999	-0.001	0.021	2.10%	1.591	1.571
		1.5	1.509	+0.009	0.032	2.14%	1.031	0.943
		2	1.965	-0.035	0.025	1.27%	1.337	0.872
		2.5	2.477	-0.023	0.027	1.11%	1.216	0.941
		3	2.973	-0.027	0.022	0.75%	1.499	1.098
		3.5	3.464	-0.036	0.021	0.61%	1.576	1.006
		4	3.975	-0.025	0.011	0.28%	3.003	2.258
		4.5	4.458	-0.042	0.015	0.34%	2.187	1.260
		5	4.949	-0.051	0.014	0.29%	2.332	1.152
0.4	Arachne	1	0.994	-0.006	0.019	1.94%	1.731	1.634
		1.5	1.494	-0.006	0.005	0.31%	7.240	6.791
		2	1.990	-0.010	0.014	0.70%	2.386	2.152
		2.5	2.502	+0.002	0.008	0.30%	4.369	4.273
		3	2.993	-0.007	0.016	0.52%	2.146	2.004
		3.5	3.493	-0.007	0.012	0.33%	2.883	2.675
		4	3.999	-0.001	0.013	0.33%	2.527	2.502
		4.5	4.500	+0.000	0.008	0.17%	4.427	4.418
		5	4.999	-0.001	0.011	0.22%	2.990	2.972
0.6	Classic	1	1.101	+0.101	0.026	2.40%	1.261	-0.018
		1.5	1.490	-0.010	0.016	1.05%	2.133	1.928
		2	1.996	-0.004	0.012	0.60%	2.790	2.684
		2.5	2.454	-0.046	0.032	1.29%	1.052	0.564
		3	2.912	-0.088	0.026	0.90%	1.277	0.156
		3.5	3.417	-0.083	0.035	1.03%	0.945	0.163
		4	3.925	-0.075	0.031	0.79%	1.081	0.273
		4.5	4.405	-0.095	0.033	0.74%	1.025	0.047
		5	4.892	-0.108	0.030	0.60%	1.129	-0.093
0.6	Arachne	1	0.952	-0.048	0.061	6.41%	0.546	0.285
		1.5	1.482	-0.018	0.027	1.83%	1.233	1.006
		2	1.972	-0.028	0.011	0.54%	3.126	2.245
		2.5	2.477	-0.023	0.030	1.20%	1.119	0.861
		3	2.980	-0.020	0.013	0.43%	2.619	2.095
		3.5	3.489	-0.011	0.009	0.26%	3.720	3.326
		4	3.985	-0.015	0.010	0.25%	3.317	2.819
		4.5	4.442	-0.058	0.025	0.56%	1.342	0.569
		5	4.964	-0.036	0.029	0.58%	1.149	0.733
0.8	Classic	1	1.432	+0.432	0.011	0.76%	3.043	-0.102
		1.5	1.508	+0.00	0.060	4.01%	0.551	0.508
		2	1.984	-0.016	0.037	1.88%	0.895	0.755
		2.5	2.429	-0.071	0.034	1.40%	0.977	0.279
		3	3.028	+0.028	0.029	0.95%	1.164	0.835
		3.5	3.436	-0.064	0.040	1.16%	0.833	0.303
		4	3.909	-0.091	0.039	0.99%	0.864	0.081
		4.5	4.447	-0.053	0.031	0.70%	1.069	0.502
		5	4.945	-0.055	0.032	0.64%	1.051	0.475
0.8	Arachne	1	0.973	-0.027	0.028	2.88%	1.188	0.872
		1.5	1.496	-0.004	0.011	0.71%	3.143	3.017
		2	1.984	-0.016	0.014	0.68%	2.459	2.061
		2.5	2.484	-0.016	0.013	0.51%	2.633	2.222
		3	2.978	-0.022	0.036	1.20%	0.936	0.732
		3.5	3.482	-0.018	0.019	0.54%	1.786	1.468
		4	3.981	-0.019	0.012	0.31%	2.671	2.158
		4.5	4.474	-0.026	0.018	0.41%	1.830	1.351
		5	4.994	-0.006	0.014	0.29%	2.330	2.195

3.4 Statistical significance

The paired t-test on absolute errors (Table 5) confirmed a statistically significant advantage for Arachne at the 0.4 mm nozzle ($p = 0.004$) and the 0.6 mm nozzle ($p = 0.011$). At the 0.8 mm nozzle the p-value rose to 0.119, missing the $\alpha = 0.05$ threshold even though the difference pointed the same way. The extreme outlier in the Classic 1 mm wall (bias +0.432 mm) drives this loss of significance: it inflates the variance of the paired differences and masks the very large mean improvement (0.091 vs. 0.017 mm). The F-test on error variances (Table 6) tells a complementary story: variances differ significantly at all three nozzle diameters ($p \leq 0.019$), with Arachne consistently the more uniform algorithm. Together, Tables 5 and 6 establish that Arachne produces both lower-magnitude and more repeatable errors than Classic across the full nozzle range tested.

Table 5

Paired t-test on absolute error (Arachne vs Classic) across 9 feature sizes, per nozzle. ***H0: mean |error| is the same for both algorithms. p<0.05 - significant difference.***

Nozzle	Mean |Err| Classic	Mean |Err| Arachne
0.4	0.0276	0.0044
0.6	0.0678	0.0285
0.8	0.0908	0.0170

Diff (A–C)	Paired t p-value	Significant?	Better algorithm
-0.0232	0.0036	Yes	Arachne
-0.0393	0.0109	Yes	Arachne
-0.0738	0.1194	No	no difference

Table 6

F-test on absolute error variance (Arachne vs Classic) across 9 feature sizes, per nozzle. H0: variances of |error| are equal between algorithms. P < 0.05 - significant difference in consistency.

Nozzle	Variance Classic	Variance Arachne	F-test p-value	More consistent
0.4	0.00025	0.00001	0.0003	Arachne
0.6	0.00152	0.00025	0.0192	Arachne
0.8	0.01709	0.00006	0.0000	Arachne

To test whether the two algorithms differ in consistency as well as in mean error, an F-test on the variance of absolute errors was performed at each nozzle diameter, with the results reported in Table 6.

3.5 Print time and material consumption

Figs. 12 and 13 summarize print time and material consumption. Print-time differences between the two algorithms were negligible (Fig. 12): Arachne took +1.2% (2 min) longer at 0.4 mm, +0.7% (1 min) longer at 0.6 mm, and −1.0% (1 min) shorter at 0.8 mm, where it ran marginally faster than Classic. Mass differences were similarly small (Fig. 13): Arachne specimens were 1.78 g heavier at 0.4 mm, 0.64 g heavier at 0.6 mm, and 1.06 g lighter at 0.8 mm. All six specimens fell roughly 22–28% short of the theoretical solid mass of 136.3 g, reflecting the 30% grid infill and the internal void fraction shared by both algorithms. The dimensional-accuracy gains reported in sections 3.1–3.4 therefore come at essentially zero cost in throughput or material, supporting Arachne as a drop-in replacement for the Classic generator in production FFF workflows.

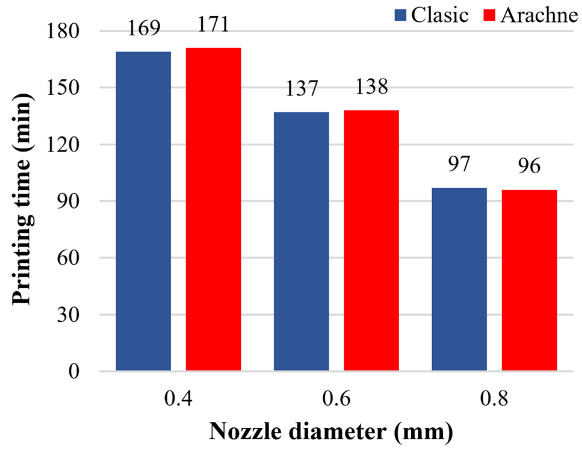

Fig. 12. Total printing time per specimen for the Classic and Arachne algorithms at each nozzle diameter.

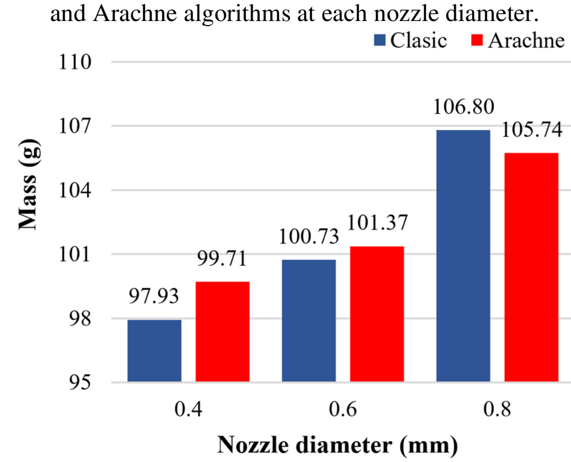

Fig. 13. Measured specimen mass for the Classic and Arachne algorithms at each nozzle diameter.

4. CONCLUSIONS

This study benchmarked the Arachne adaptive bead-width algorithm against the Classic uniform-offset algorithm for FFF on a custom L-shaped wall geometry printed at three nozzle diameters (0.4, 0.6, 0.8 mm) on a Bambu Lab A1 in PolyTerra PLA, evaluating dimensional accuracy, precision, and efficiency. Five conclusions follow:

(1) Arachne reduced the mean absolute error by 2.3 to 7.0 times compared to the Classic algorithm across all nozzle diameters, with the largest improvements observed at 0.4 mm nozzle (MAE 0.004 vs. 0.028 mm) and 0.8 mm nozzle (MAE 0.017 vs. 0.091 mm).

(2) All 27 feature measurements (9 features × 3 nozzles) printed with Arachne fell within ±0.1 mm of the nominal dimension, whereas the Classic algorithm exceeded this tolerance for 3 out of 27 features, with the most severe case being the 1 mm wall at 0.8 mm nozzle (+0.432 mm bias).

(3) The Arachne regression slope held within 0.2% of unity at every nozzle size (range 0.999–1.002), while the Classic slope drifted from 0.989 at 0.4 mm to 0.924 at 0.8 mm, confirming a systematic scaling error that worsens with nozzle diameter.

(4) These accuracy gains came at negligible cost: print time differed by no more than ±1.2% and material consumption by no more than ±1.8%, qualifying Arachne as a direct drop-in replacement for Classic in any FFF workflow.

(5) Arachne reduced the variance of dimensional errors significantly across all nozzle sizes (F-test $p \leq 0.019$), delivering not only higher accuracy but also more predictable, process-capable printing.

These physical measurements validate the computational predictions of Kuipers et al. (2020) and extend them to a commercial direct-drive FFF platform. Future work should evaluate Arachne with engineering thermoplastics (e.g., PETG, ABS, PA), at varying layer heights, and on geometries featuring curved walls and thin-walled lattice structures.

5. REFERENCES

[1] Kuipers, T., Doubrovski, E.L., Wu, J., Wang, C.C.L., A framework for adaptive width control of dense contour-parallel toolpaths in fused deposition modeling. Comput. Aided Des. 128, 102907, 2020. DOI: 10.1016/j.cad.2020.102907

[2] Ngo, T.D., Kashani, A., Imbalzano, G., Nguyen, K.T.Q., Hui, D., Additive manufacturing (3D printing): A review of materials, methods, applications and challenges. Compos. Part B Eng. 143, 172–196, 2018. DOI: 10.1016/j.compositesb.2018.02.012

[3] Ermolai, V., Rîpanu, M.-I., Merticaru, V. Jr., Irimia, A.-I., Mihalache, M.-A., Sover, A., Mititelu, N.-R., Pișta, I.-M., XYZ calibration cube – A misleading tool for achieving print accuracy. Mater. Res. Proc. 46, 23–34, 2024. DOI: 10.21741/9781644903377-4

[4] Sood, A.K., Ohdar, R.K., Mahapatra, S.S., Improving dimensional accuracy of fused deposition modelling processed part using grey Taguchi method. Mater. Des. 30, 4243–4252, 2009. DOI: 10.1016/j.matdes.2009.04.030

[5] Górski, F., Kuczko, W., Wichniarek, R., Influence of process parameters on dimensional accuracy of parts manufactured using fused deposition modelling technology. Adv. Sci. Technol. Res. J. 7(19), 27–35, 2013. DOI: 10.5604/20804075.1062340

[6] Jiang, J., Ma, Y., Path planning strategies to optimize accuracy, quality, build time and material use in additive manufacturing: A review. Micromachines 11(7), 633, 2020. DOI: 10.3390/mi11070633

[7] Ermolai, V., Irimia, A., Influence of nozzle parameters in 3D printing under the manufacturing time. Bull. Polytech. Inst. Iași Mach. Constr. Sect. 67, 63–72, 2021.

[8] Sun, Q., Mazur, A., Cheng, J., A review of void reduction strategies in material extrusion-based additive manufacturing. Addit. Manuf. 67, 103463, 2023. DOI: 10.1016/j.addma.2023.103463

[9] Altıparmak, S.C., Yardley, V.A., Shi, Z., Lin, J., Extrusion-based additive manufacturing technologies: State of the art and future perspectives. J. Manuf. Process. 83, 607–636, 2022. DOI: 10.1016/j.jmapro.2022.09.032

[10] Hornus, S., Kuipers, T., Devillers, O., Teillaud, M., Martínez, J., Glisse, M., Lazard, S., Lefebvre, S., Variable-width contouring for additive manufacturing.

ACM Trans. Graph. 39(4), 130, 2020. DOI: 10.1145/3386569.3392448

[11] Xiong, Y., Park, SI., Padmanathan, S., Dharmawan, AG., Foong, S., Rosen, DW., Soh, GS., Process planning for adaptive contour parallel toolpath in additive manufacturing with variable bead width. Int. J. Adv. Manuf. Technol. 105, 4159–4170, 2019. DOI: 10.1007/s00170-019-03954-1

[12] Kuipers, T., Wu, J., Wang, C.C.L., CrossFill: Foam structures with graded density for continuous material extrusion. Comput. Aided Des. 114, 37–50, 2019. DOI: 10.1016/j.cad.2019.05.003

[13] Mohamed, O.A., Masood, S.H., Bhowmik, J.L., Optimization of fused deposition modeling process parameters: A review of current research and future prospects. Adv. Manuf. 3(1), 42–53, 2015. DOI: 10.1007/s40436-014-0097-7

[14] Allum, J., Moetazedian, A., Gleadall, A., Mitchell, N., Marinopoulos, T., McAdam, I. & Silberschmidt, VV., Extra-wide deposition in extrusion additive manufacturing: A new convention for improved interlayer mechanical performance. Addit. Manuf. 61, 103334, 2023. DOI: 10.1016/j.addma.2022.103334.

Generarea perimetrelor adaptive pentru fabricarea cu filament fuzionat: evaluarea algoritmului Arachne

Rezumat: În fabricația filament fuzionat (FFF), precizia dimensională este influențată semnificativ de strategia de depunere perimetrală. Algoritmul de secționare Arachne variază lățimea de extrudare de-a lungul fiecărui perimetru printr-o strategie de profilare pe axa mediană, adaptându-se la geometria locală a peretelui, în timp ce algoritmul Classic menține lățimea conturului fixă. Astfel, au fost comparat experimental cei doi algoritmi de secționare pe un model de referință în formă de L special conceput, cu grosimi ale pereților de la 1 la 5 mm, imprimat cu trei duze cu diametre diferite (0,4, 0,6 și 0,8 mm) pe un Bambu Lab A1 cu PolyTerra PLA. În urma celor 270 de măsurători cu micrometrul, a rezultat că Arachne a redus eroarea absolută medie de 2,3 până la 7,0 ori și a menținut 100% din caracteristici în limita a ±0,1 mm față de valoarea nominală pentru toate cel trei diametre ale duzelor, în timp ce algoritmul Classic a atins doar 78% (0,6 mm) și 89% (0,8 mm). Diferențele de timp de imprimare și de consum de material au rămas sub 1,2% și, respectiv, 1,8%, confirmând costuri de producție neglijabile.

Alexandru Ionuț IRIMIA, PhD. student, "Gheorghe Asachi" Technical University of Iasi, Faculty of Machine Manufacturing and Industrial Management, Iași, Romania, email: alexandru-ionut.irimia@student.tuiasi.ro.

Ionuț Mădălin PIȘTA, PhD. Eng., Aumovio Technologies Romania SRL, Iasi, Romania, ionut-madalin.pista@aumovio.com

Marius Ionuț RÎPANU, PhD. Associate Professor, Eng., "Gheorghe Asachi" Technical University of Iasi, Faculty of Machine Manufacturing and Industrial Management, Iași, Romania, email: marius-ionut.ripanu@academic.tuiasi.ro

Vasile MERTICARU, PhD. Associate Professor, Eng., "Gheorghe Asachi" Technical University of Iasi, Faculty of Machine Manufacturing and Industrial Management, Iași, Romania, email: vasile.merticaru@academic.tuiasi.ro

Marius-Andrei MIHALACHE, PhD. Associate Professor, Eng. "Gheorghe Asachi" Technical University of Iasi, Faculty of Machine Manufacturing and Industrial Management, Iași, Romania, email: marius-andrei.mihalache@academic.tuiasi.ro

Vasile ERMOLAI, PhD. Assistant Professor, Eng., "Gheorghe Asachi" Technical University of Iasi, Faculty of Machine Manufacturing and Industrial Management, Iași, Romania, email: vasile.ermolai@academic.tuiasi.ro